Appl Microbiol Biotechnol
DOI 10.1007/s00253-017-8450-y

BIOTECHNOLOGICALLY RELEVANT ENZYMES AND PROTEINS

# 2′-Deoxyribosyltransferase from *Leishmania mexicana*, an efficient biocatalyst for one-pot, one-step synthesis of nucleosides from poorly soluble purine bases

**N. Crespo[1,2] · P. A. Sánchez-Murcia[3,4] · F. Gago[4] · J. Cejudo-Sanches[2] · M. A. Galmes[2] · Jesús Fernández-Lucas[2,5] · José Miguel Mancheño[1]**

Received: 18 May 2017 / Revised: 19 July 2017 / Accepted: 21 July 2017


**Abstract** Processes catalyzed by enzymes offer numerous advantages over chemical methods although in many occasions the stability of the biocatalysts becomes a serious concern. Traditionally, synthesis of nucleosides using poorly water-soluble purine bases, such as guanine, xanthine, or hypoxanthine, requires alkaline pH and/or high temperatures in order to solubilize the substrate. In this work, we demonstrate that the 2′-deoxyribosyltransferase from *Leishmania mexicana* (*Lm*PDT) exhibits an unusually high activity and stability under alkaline conditions (pH 8–10) across a broad range of temperatures (30–70 °C) and ionic strengths (0–500 mM NaCl). Conversely, analysis of the crystal structure of *Lm*PDT together with comparisons with hexameric, bacterial homologs revealed the importance of the relationships between the oligomeric state and the active site architecture within this family of enzymes. Moreover, molecular dynamics and docking approaches provided structural insights into the substrate-binding mode. Biochemical characterization of *Lm*PDT identifies the enzyme as a type I NDT (PDT), exhibiting excellent activity, with specific activity values 100- and 4000-fold higher than the ones reported for other PDTs. Interestingly, *Lm*PDT remained stable during 36 h at different pH values at 40 °C. In order to explore the potential of *Lm*PDT as an industrial biocatalyst, enzymatic production of several natural and non-natural therapeutic nucleosides, such as vidarabine (ara A), didanosine (ddI), ddG, or 2′-fluoro-2′-deoxyguanosine, was carried out using poorly water-soluble purines. Noteworthy, this is the first time that the enzymatic synthesis of 2′-fluoro-2′-deoxyguanosine, ara G, and ara H by a 2′-deoxyribosyltransferase is reported.

**Keywords** 2′-deoxyribosyltransferase · Enzymatic synthesis · Industrial biocatalyst · Protein crystallography · Molecular docking · Purine nucleoside analogues

N.C and P.A.S-M contributed equally to this work.

**Electronic supplementary material** The online version of this article (doi:10.1007/s00253-017-8450-y) contains supplementary material, which is available to authorized users.

✉ Jesús Fernández-Lucas
jesus.fernandez2@universidadeuropea.es

✉ José Miguel Mancheño
xjosemi@iqfr.csic.es

[1] Department of Crystallography and Structural Biology, Institute Rocasolano (CSIC), Serrano 119, E-28006 Madrid, Spain

[2] Applied Biotechnology Group, European University of Madrid, E-28670 Villaviciosa de Odón, Madrid, Spain

[3] Institute of Theoretical Chemistry, Faculty of Chemistry, University of Vienna, 1090 Vienna, Austria

[4] Department of Biomedical Sciences and "Unidad Asociada IQM-CSIC", School of Medicine and Health Sciences, University of Alcalá, E-28871 Alcalá de Henares, Spain

[5] Grupo de Investigación en Desarrollo Agroindustrial Sostenible, Department of Agroindustrial Engineering, School of Environmental Sciences, Universidad de la Costa, Cra. 55 #58-66, Barranquilla, Colombia

## Introduction

Nucleic acid derivatives (NADs) such as nucleosides, nucleotides, or nucleobases are known to be ubiquitous molecules in biochemical processes of storage and genetic transfer of the information. Besides, the therapeutic potential and applicability of many NADs to treat diseases or their use as building blocks in the synthesis of oligonucleotides is well known (De Clerq 2005a, b; Galmarini et al. 2002; Parker 2009; Robak et al. 2006). Therefore, many efforts have been made over the

years to improve the synthetic methods to obtain NADs. Conventionally, these molecules have been synthesized by chemical methods, which often require time-consuming multistep processes, including protection–deprotection strategies or the use of chemical reagents and organic solvents that are expensive and environmentally harmful (Boryski 2008). In contrast, the alternative enzymatically based approaches for the synthesis of NADs have gained relevance due to the easy implementation of one-pot one-step reactions under mild conditions or environmentally friendly conditions (Lewkowicz and Iribarren 2006; Mikhailopulo 2007; Fresco-Taboada et al. 2013). Hence, the replacement of chemical synthesis by enzymatic or chemo-enzymatic strategies in the industrial synthesis of NADs is frequently observed. In this respect, microbial nucleoside phosphorylases (NPs) and *N*-deoxyribosyltransferases (NDTs) are extensively used in the synthesis of natural and non-natural nucleosides as biocatalyst for the transfer of glycosyl residues to acceptor bases (Fresco-Taboada et al. 2013).

*N*-deoxyribosyltransferases (EC 2.4.2.6) catalyze the direct transfer of the 2-deoxyribosyl moiety from a 2′-deoxynucleoside donor to a nucleobase acceptor through a one-step reaction (Fresco-Taboada et al. 2013; Kaminski 2002). Nucleoside 2′-deoxyribosyltransferases are classified into two classes depending on their substrate specificity: type I (PDT), which are specific for purines (Pur↔Pur) and type II (NDT), which catalyzes the transfer between purines and/or pyrimidines (Pur↔Pur, Pur↔Pyr, Pyr↔Pyr) (Fresco-Taboada et al. 2013; Fernández-Lucas et al. 2010). Although NDTs are regio- (N-1 glycosylation in pyrimidine and N-9 in purine) and stereoselective (exclusively the β-anomers are formed) enzymes for 2′-deoxyribonucleosides, recent studies have revealed that some NDTs can recognize substrates containing modifications at positions 2′C and 3′C of the deoxyribose moiety (Fresco-Taboada et al. 2013; Kamisnki et al. 2008).

Enzymatic synthesis of natural and non-natural nucleosides using poorly water-soluble purine bases is hindered by the low solubility of some purines, such as guanine, hypoxanthine, or xanthine, which may cause underperformance of the biocatalyst (Yokozeki and Tsuji 2000; Okuyama et al. 2003). Traditionally, to circumvent this limitation, high temperature and alkaline conditions were used, resulting in a higher solubilization of substrates, a diminution of medium-viscosity, and an increase of substrate diffusion coefficients, leading to higher overall reaction rate. Unfortunately, neither PDT nor NDT enzymes exhibit high catalytic activities under basic pH values or high temperatures. Okuyama et al. (2003) have applied a smart approach by coupling the production 2,6-diaminopurine-2′-deoxyriboside by the NDT from *Lactobacillus helveticus* (*Lh*NDT) with a bacterial adenosine deaminase (*Ec*ADA) for the ensuing hydrolytic step to obtain 2′-deoxyguanosine (dGuo) in high yields. Complementarily, the addition of water-miscible organic solvents to the reaction media to improve the solubility of guanine has been described (Yokozeki and Tsuji 2000; Müller et al. 1996). As an example, we have recently reported the effect of several water-miscible co-solvents on the activity and stability of free and immobilized 2′-deoxyribosyltransferase from *Lactobacillus reuteri* in order to establish the optimal conditions for enzymatic synthesis of nucleosides using poorly water-soluble purine bases (Fernández-Lucas et al. 2012).

Here, we have carried out thorough structural and biochemical studies of the 2′-deoxyribosyltransferase type I from *Leishmania mexicana* (*Lm*PDT). Structurally, the comparison of the dimeric assembly of *Lm*PDT with bacterial, hexameric homologs has revealed unexpected features of the active site architecture of these enzymes. Conversely, as a biocatalyst, *Lm*PDT presents significant stability and catalytic activity under alkaline and high temperature experimental conditions, displaying high activity values compared to other reported PDTs (Kaminski 2002; Lawrence et al. 2009). These unusual catalytic properties together with the promiscuity in the recognition of the sugar moiety showed by *Lm*PDT allowed the synthesis of different purine nucleoside analogues from poorly soluble purine bases. To the best of our knowledge, this is the first time that enzymatic synthesis of ara G, ara H, and 2′-fluoro-2′-deoxyguanosine is reported by using a 2′-deoxyribosyltransferase as catalyst.

## Materials and methods

### Reagents

Cell culture medium reagents were from Difco (St. Louis, MO). Trimethylammonium acetate buffer were purchased from Sigma-Aldrich. All other reagents and organic solvents were purchased to Scharlab (Barcelona, Spain) and Symta (Madrid, Spain). All NADs (nucleosides and nucleobases) used in this work were provided by Carbosynth Ltd. (Compton, UK).

### Gene cloning and expression and protein production and purification

The synthetic *pdt* gene encoding the putative PDT from *L. mexicana* (European Nucleotide Archive code: CBZ27326.1; UniProtKB code E9AWJ0) was ordered and purchased from Genscript (USA). The coding sequence appeared as a *Nde*I-*Eco*RI fragment subcloned into the expression vector pET28b(+). The resultant, recombinant vector pET28b*LmPDT* provided the corresponding N-terminal $His_6$-tagged fusion protein with a thrombin cleavage site between the tag and the enzyme. The recombinant enzyme was produced in *Escherichia coli* BL21(DE3) grown in LB medium at 37 °C with kanamycin 50 μg/mL. Protein

overexpression was induced by adding 0.5 mM isopropil-β-D-1-thiogalactopyranoside and the cells further grown for 3 h. The cells were harvested via centrifugation at 3500×*g*. The resulting pellet was resuspended in Tris buffer (20 mM Tris-HCl, pH 8.0, containing 100 mM NaCl). Crude extracts were prepared by French press lysis of cell suspensions. The lysate was centrifuged at 17500×*g* for 40 min and the supernatant was filtered through a 0.22-μm filter (Millipore). The cleared lysate was then loaded onto a 5-mL HisTrap FF column (GE Healthcare) pre-equilibrated in a binding buffer (20 mM Tris-HCl buffer, pH 8.0, with 100 mM NaCl and 10 mM imidazole) and the column was washed. Bound proteins were eluted using a linear gradient of imidazole (from 10 to 500 mM). Fractions containing *Lm*PDT were identified by SDS-PAGE, pooled, concentrated, and loaded onto a HiLoad 16/60 Superdex 200 prep grade column (GE Healthcare) pre-equilibrated in Tris buffer. Fractions with the protein of interest identified by SDS-PAGE were pooled and the protein was concentrated and stored at −80 °C until its use. Protein concentration was determined spectrophotometrically by UV absorption at 280 nm using a $\varepsilon_{280}$ = 34,380 $M^{-1}$ $cm^{-1}$ (Gill and Von Hippel 1989).

### N-deoxyribosyltransferase assay

The standard enzymatic activity assay was performed in a final volume of 40 μL by addition to the pure enzyme (0.3 μg of in 50 mM MES buffer, pH 6.5) the substrate (dGuo or Ade 10 mM in 50 mM MES buffer, pH 6.5) for 5 min at 40 °C (30 rpm). The enzymatic reaction was quenched by addition of 40 μL of cold methanol in ice-bath and heated for 5 min at 95 °C as described previously (Fernández-Lucas et al. 2010; Fernández-Lucas et al. 2012). After centrifugation at 9000×*g* for 2 min, samples were half-diluted with water and the nucleoside production was analyzed by HPLC to quantitatively measure the reaction products as described below in the analytical methods. All determinations were carried out by triplicate and the maximum error was below 5%. In such conditions, one international activity unit (IU) was defined as the amount of enzyme producing 1 μmol/min of 2′-deoxyadenosine under the assay conditions.

### Analytical methods

Production of nucleosides was analyzed quantitatively with an ACE 5 μm C18-PFP column 250 mm × 46 mm (Advanced Chromatography Technologies) pre-equilibrated in 100% trimethyl ammonium acetate. Elution was carried out by a discontinuous gradient, 0–10 min, 100 to 90% trimethyl ammonium acetate and 0 to 10% acetonitrile, and 10–20 min, 90 to 100% trimethyl ammonium acetate and 10 to 0% acetonitrile. Retention times for the reference natural compounds (hereafter abbreviated according to the recommendations of the IUPAC-IUB Commission on Biochemical Nomenclature) were as follows: adenine (Ade): 10.14 min; 2′-deoxyadenosine (dAdo), 15.50 min; guanine (Gua), 8.1 min; 2′-deoxyguanosine (dGuo), 12.8 min; hypoxanthine (Hyp), 7.5 min; and 2′-deoxyinosine (dIno), 12.1 min. Retention times for the reference non-natural compounds (hereafter abbreviated according to the recommendations of the IUPAC-IUB Commission on Biochemical Nomenclature) were as follows: ara adenine (ara A), 14.0 min; ara guanine (ara G), 11.4; ara hypoxantine (ara H), 11.0; 2′-deoxy-2′-fluoroadenosine (2′dFAdo), 17.0; 2′-deoxy-2′-fluoroguanosine (2′dFGuo), 13.6; 2′-deoxy-2′-fluoroinosine (2′dFIno), 13.3; 2′,3′-dideoxyadenosine (ddA), 19.0 min; 2′,3′-dideoxyiguanosine (ddG), 15.3 min; and 2′,3′-dideoxyinosine (ddI), 14.8 min.

### Biochemical characterization

The optimal temperature for enzyme activity was determined by measuring the activity of *Lm*PDT between 20 and 90 °C using the *N*-deoxyribosyltransferase assay. The optimal pH for enzyme activity was also determined by measuring the activity in the pH range from 4 to 10, incubating 0.3 μg of pure enzyme with 10 mM 2′-deoxyguanosine (dGuo) and 10 mM adenine (Ade) in different reaction buffers (sodium citrate, pH 4–6; sodium phosphate, pH 6–8; sodium borate, pH 8–10) using standard reaction conditions. A similar approach has been followed to characterize the effect of ionic strength on enzyme activity. *Lm*PDT activity has been measured at different concentrations of NaCl, ranging from 0 to 1000 mM.

The thermal stability of *Lm*PDT was studied by incubating enzyme solutions (60 μg/ml in 50 mM MES buffer, pH 6.5, or in 50 mM sodium borate buffer, pH 8.5), at temperatures ranging from 40 to 50 °C. At regular intervals, 5 μL aliquots were withdrawn from the incubation mixture and the residual activity was determined at 40 °C using dAdo synthesis from dGuo and Ade under the standard assay conditions.

### Enzymatic synthesis of natural and non-natural purine nucleosides from low soluble water purine bases

Enzymatic synthesis of natural nucleosides was performed as described for *N*-deoxyribosyltransferase assay using different purine 2′-deoxyribonucleosides and bases (10 mM). Enzymatic synthesis of non-natural nucleosides was carried out incubating 3.0 μg of *Lm*PDT with modified purine nucleosides (arabinosyl nucleosides, 2′-deoxy-2′-fluoronucleosides and 2′,3′-dideoxyribosylnucleosides) and natural purine bases at different conditions.

### Enzyme crystallization and data collection

Crystallization of *Lm*PDT (15 mg/mL in Tris buffer) was performed on VDX hanging drop plates (Hampton Research) at

JnlID 253_ArtID 8450_Proof# 1 - 29/07/2017



291 K. Crystal plates grew in 25% PEG 3350, 0.2 M magnesium chloride, 0.1 M Tris-HCl, pH 8.5 (protein/precipitant drop ratio 2:1) by vapor diffusion.

For diffraction data collection, *Lm*PDT crystals were transferred to an optimized cryoprotectant solution consisting of mother liquor plus 20% (*v/v*) glycerol before being cooled to 100 K in a cold nitrogen-gas stream. Diffraction data were collected on beamline BL13-XALOC at the ALBA synchrotron (Barcelona, Spain) with a Pilatus 6M detector (Area Detector Systems Corp.) and a crystal-to-detector distance of 242.38 mm. A total of 1440 images were collected with a 0.25° oscillation angle. Diffraction images were processed with *XDS* (Kabsch 2010) and the space group examination was performed with *POINTLESS* (Evans 2011). Crystals of *Lm*PDT belonged to the monoclinic space group *C*2, with two molecules in the asymmetric unit and 36% solvent content within the unit cell. A summary of data collection statistics is provided in Table 1.

**Table 1** Data collection and refinement statistics

| *Lm*PDT | |
|---|---|
| PDB code | 5NBR |
| Data collection | |
| Synchrotron source | ALBA |
| Beamline | BM13-XALOC |
| Wavelength (Å) | 0.9793 |
| Space group | *C*2 |
| Unit-cell parameters | $a$ = 80.2, $b$ = 46.3, $c$ = 87.9 $\alpha$ = 90°, $\beta$ = 115.1°, $\gamma$ = 90° |
| Resolution range (Å) | 39.85–1.66 |
| No. of measured reflections[a] | 228,772 (11,234) |
| No. of unique reflections | 33,859 (1595) |
| Mean ($I/\sigma I$) | 18.3 (3.1) |
| Completeness (%) | 97.7 (96.4) |
| Multiplicity | 6.8 (7.0) |
| $R_{meas}$ (%); $R_{pim}$ (%) | 5.2 (64.5); 2.8(33.8) |
| *B*-factor (Wilson plot, Å$^2$) | 25.8 |
| Molecules/non-H atoms | |
| Protein | 2/2639 |
| Water | 250/250 |
| Refinement statistics | |
| $R_{work}$ (%)/$R_{free}$ (%) | 16.8/20.3 |
| Average B-factors (Å$^2$) | |
| Protein | 31.7 |
| Water | 35.2 |
| Rms deviation bond length (Å) | 0.007 |
| Rms deviation angles (°) | 0.788 |
| Ramachandran | |
| Favored (%) | 95.4 |
| Disallowed (%) | 0.33 |

[a] Values for the highest resolution shell are given in parentheses

## Structure solution and refinement

The structure of *Lm*PDT was solved by molecular replacement using *phenix.phaser* (McCoy 2007). The atomic coordinates of nucleoside 2′-deoxyribosyltransferase from *Trypanosoma brucei* were used as search model (*Tb*NDT; PDB entry 2A0K). Model rebuilding was performed manually using *COOT* (Emsley et al. 2010) and refinement was carried out with *phenix.refine* (Afonine et al. 2012) in PHENIX (Adams et al. 2010). Refinement steps included *xyz* refinement, TLS, individual atomic displacement parameters (ADPs), addition of ligands, and solvent molecules. The refined structure has a final *R*-factor of 16.8% ($R_{free}$ = 20.5%) for data up to 1.66 Å. Analysis of the interfacial surfaces was done with the PISA server (Krissinel and Henrick 2007). Analysis of the secondary structure was done with DSSP (Touw et al. 2015). Stereochemistry validation was done with the Phenix MolProbity tool plus de wwPDB Deposition server. PyMOL (DeLano 2002) was used for structure visualization and figure preparation. Data collection and refinement statistics are listed in Table 1.

## Computational methods

Optimized geometries of the complex *Lm*PDT with 2′-deoxyadenosine (dAdo) and Glu85-ribosylated form of the enzyme were achieved following a restrained molecular dynamics (MD) protocols using the Amber14 suite of programs (Case et al. 2014). The X-ray crystal structure of *L. helveticus* purine 2′-deoxyribosyltransferase (*Lh*PDT) in complex with dAdo (PDB entry 1S2G (Anand et al. 2004) was superimposed onto the crystal structure of *Lm*PDT with PyMOL (DeLano 2002) and dAdo was manually docked into the binding site. Geometry optimization of dAdo and the ribosylated Glu85 was achieved in vacuo using the RESP ESP charge Derive Server (Vanquelef et al. 2011) following the standard procedure. The input files for dAdo and the ribosylated Glu85 were generated using the *anterchamber* utility included in the AMBER14 suite (Case et al. 2014).

The conformation of the loop 43-46 of *Lm*PDT in the presence of dAdo was modeled by means of unrestrained MD simulations at 300 K and 1 atm. All the positions of the Cα atoms of the protein, except those of the former loop, were restrained by imposing a harmonic force constant of 5 kcal mol$^{-1}$ Å$^{-2}$. In all systems, the protein was immersed in a box of ~ 17,000 TIP3P water molecules that extended 25 Å away from any solute atom and 12 $Na^+$ ions were added to ensure electrical neutrality. The MD simulation was carried out as described before (Sánchez-Murcia et al. 2016) using the *pmemd_cuda.SPFP* module and the standard ff14SB force field parameter set in AMBER14. Our in-house MM-ISMSA program (Klett et al. 2012) was then employed on a set of 150 snapshots from the MD trajectory of the *Lm*PDT/dAdo

complex to calculate the solvent-corrected binding energies at the dimer interface of the protein. The affinity maps were computed with program cGRILL (Cortés-Cabrera et al. 2015).

### Analytical ultracentrifugation

Sedimentation velocity for *Lm*PDT were carried out in 20 mM Tris-HCl, pH 8.0 at 20 °C and 50,000×*g* in an Optima XL-I analytical ultracentrifuge (Beckman-Coulter Inc.), equipped with UV-VIS absorbance and Raleigh interference detection systems, using an An-60Ti rotor and standard (12-mm optical path) double-sector center pieces of Epon-charcoal. Sedimentation profiles were recorded at 292 nm. Sedimentation coefficient distributions were calculated by least-squares boundary modeling of sedimentation velocity using the continuous distribution *c(s)* Lamm equation model as implemented by SEDFIT 14.7g.

Baseline offsets were measured afterwards at 200,000×*g*. The apparent sedimentation coefficient of distribution, *c*(*s*), and sedimentation coefficient s were calculated from the sedimentation velocity data using the program SEDFIT (Brown and Schuck 2006). The experimental sedimentation coefficients were corrected to standard conditions (water, 20 °C, and infinite dilution) using the software SEDNTERP (Laue et al. 1992) to get the corresponding standard s values ($s_{20,w}$).

### Accession number

The atomic coordinates and structure factors have been deposited in the Protein Data Bank with the accession code: 5NBR.

## Results

### Crystallization and structural characterization of *Lm*PDT

Optimized crystals of *Lm*PDT were grown by mixing *Lm*PDT (15 mg/mL in 20 mM Tris-HCl, 0.1 M NaCl pH 8.0) with 25% PEG 3350, 0.2 M magnesium chloride, 0.1 M Tris-HCl, and pH 8.5 (protein/precipitant drop ratio 2:1). The high-resolution crystal structure of *Lm*PDT has been determined by molecular replacement using the structure of nucleoside 2′-deoxyribosyltransferase from *T. brucei* (*Tb*NDT; PDB entry 2A0K) as a search model. The asymmetric unit contained two polypeptide chains with identical structures (the r.m.s.d. for 150 Cα positions is 0.41 Å) that are associated forming a dimeric assembly (see below). The final, refined model of the structure included chain A residues 1–154 and chain B residues 4–153. The $2F_o$-$F_c$ electron density map showed continuous density for the whole protein, excluding the side chains of chain A residues 43–46, which are located in the β2-α3 connecting loop in close proximity to the crystallographic twofold symmetry axis. All residues occupy favorable regions of the Ramachandran plot. Data collection and refinement statistics are shown in Table 1.

The *Lm*PDT subunit is a highly asymmetric α/β protein composed of a globular core and a large region situated between β4 strand and α6 helix comprised by residues 102–137, which is herein defined as the intersubunit zone (Fig. 1). The core of the structure is composed of a central, parallel, four-stranded β-sheet (with 2134 topology) with two helices packed against each of its sides (α2-α6 and α3-α4, respectively) and a helix turn (α1). Conversely, the intersubunit zone protrudes from the core towards the accompanying subunit and contains two small β-strands (β5 and β6) and an additional helix turn (α5).

The hydrodynamic behavior of *Lm*PDT studied by sedimentation velocity experiments showed that the enzyme behaves as a single species in solution with an experimental sedimentation coefficient of 3.13 S ($s_{20,w}$ = 3.15) compatible with a globular species of 37 kDa. This agrees well with a dimeric assembly of *Lm*PDT (theoretical mass of the monomer 18,706 Da), which is precisely the assembly observed in the *Lm*PDT crystal. The analysis of the protein packing of this crystal with the PISA server (Krissinel and Henrick 2007) reveals a large contacting interface between subunits (~ 4500 Å$^2$) that mainly involves residues from helices α3, α4, and α6 from the globular core, and β6 strand from the intersubunit zone. Each α6 helix becomes sandwiched between helices α3# and α4# (# indicates structural elements from the accompanying subunit) and β6 strand rests above α1#. Some residues from the large β6-α6 connecting loop (residues 120–140), and α6 helix of one subunit form part of the substrate-binding pocket of the other subunit, which explains that the dimeric assembly is the minimum catalytic unit of these enzymes (Armstrong et al. 1996). In agreement with this, the hexameric assemblies observed in the bacterial homologs (see below) 2′-deoxyribosyltransferase from *Lactobacillus leichmannii* (*Ll*NDT) (Armstrong et al. 1996) and 2′-deoxyribosyltransferase type I from *L. helveticus* (*Lh*PDT) (Anand et al. 2004) are trimers of dimers.

The global energy of interaction of the dimer interface was analyzed in silico and decomposed by residue using the approach MM-ISMSA (Klett et al. 2012). In Table S1 are listed those residues that contribute the most to the stability of the dimer along a molecular dynamics (MD) protocol where all the alpha-carbon have been positional restrained (see section Computational methods in Material and methods). Although the interaction between the C-terminal carboxylate moiety of Leu153 and the side chain of Lys5# has the large contribution, the interactions of the side chains of residues located on α4 helix (Arg74, Phe84, Tyr88) with residues on β6# strand and α6# helix (Met130, Leu118, Ser119, Ile131) are also relevant.

Structural similarity searches using the FATCAT (Ye and Godzik 2003) and DALI Lite v3 (Holm and Rosenström 2010) servers reveal *Tb*NDT as the closest structural homolog of

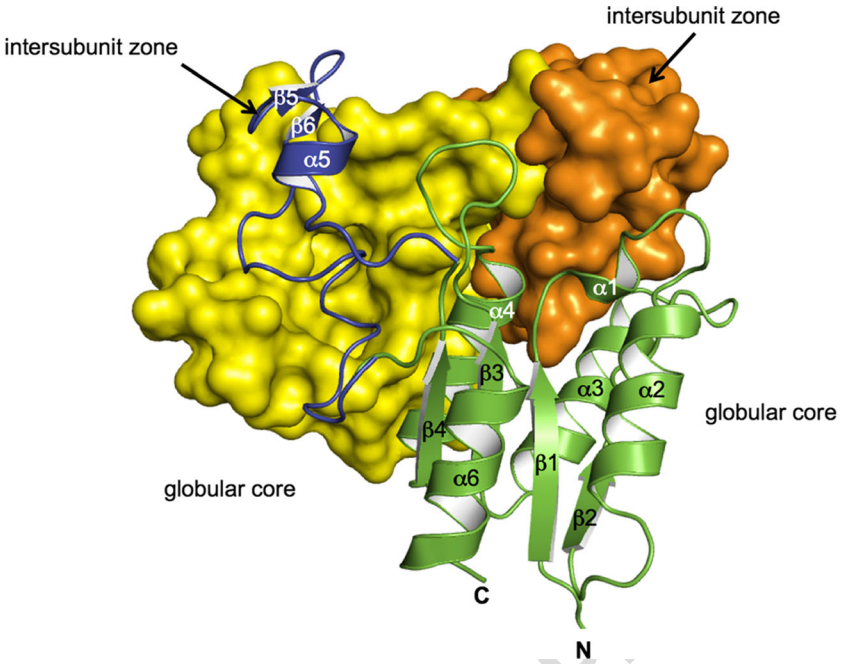


**Fig. 1** Representation of the dimeric assembly of the 2′-deoxyribosyltransferase *Lm*PDT. One subunit of the dimer is shown as the *surface* model (*yellow* corresponds to the globular core and *orange* to the intersubunit zone) and the other one as the *cartoon* model (*green* for the globular core and *blue* for the intersubunit zone). The core of each subunit is composed of a central, parallel, four-stranded β-sheet with two helices packed against each of its sides (α2-α6 and α3-α4, respectively), and a helix turn (α1). The intersubunit zone contains the β-strands β5 and β6 and an additional helix turn (α5). The regular secondary structural elements of the cartoon model are labeled. The figure has been prepared with PyMOL (DeLano 2002)



*Lm*PDT (r.m.s.d. of 1.04 Å for 150 Cα atoms and a sequence identity of 63%) followed by 2′-deoxyribosyltransferase *Ll*NDT (r.m.s.d. of 3.22 Å for 170 Cα atoms and a sequence identity of 18%; PDB entry 1F8Y) and *Lh*PDT (r.m.s.d. of 3.17 Å for 170 Cα atoms and a sequence identity of 13%; PDB entry 1S2D). A similar result is obtained using the Dali Lite v3.0 server (Holm and Rosenström 2010) but in this case also appeared the putative nucleoside 2-deoxyribosyltransferase from *Enterococcus faecalis* (sequence identity of 22%; PDB entry 3EHD).

## Architecture of the active site

The substrate-binding pocket of *Lm*PDT is made up of residues contributed by the two interacting subunits. This feature is a signature of 2′-deoxyribosyltransferases (Fresco-Taboada et al. 2013; Armstrong et al. 1996; Anand et al. 2004). The catalytic Glu85, which occupies an equivalent position to Glu82, Glu101, and Glu98 in *Tb*NDT, *Lh*PDT and *Ll*NDT, respectively (Fig. 2), is located deep inside this pocket and hydrogen bonds through its side chain with the OH atom of the Tyr8 side chain. Theoretical computation of the protonation state of the protein at pH 7.5 with the H++ server (Anandakrishnan et al. 2012) shows that Glu85 may be protonated in the unbound state as was previously suggested by Short and co-workers in PDTs of *Lactobacilli* species (Short et al. 1996). By comparison with *Lh*PDT and *Ll*NDT, it can be inferred that the residues of *Lm*PDT that participate in substrate binding are Asn56, Asp79, Thr82, and Asn128# (Fresco-Taboada et al. 2013; Armstrong et al. 1996; Anand et al. 2004). Interestingly, Asn56 (Asn53 in *Tb*NDT) is replaced by aspartic acid in *Lh*PDT and *Ll*NDT (Fig. 2). Conversely, although in the active site of *Lm*PDT several hydrophobic residues can be identified (Phe15, Ile60, Met281B), the contribution of aromatic residues is limited to Phe15 (equivalent to Tyr17 in *Lh*PDT or Phe13 in *Ll*NDT), which contrasts to *Lh*PDT and *Ll*NDT that possess several aromatic residues (Phe16, Tyr17, and Phe45 in *Lh*PDT; Trp12, Phe13, and Tyr21 in *Ll*NDT) (Armstrong et al. 1996; Anand et al. 2004).

The detailed analysis of the dimeric complexes of *Lm*PDT or *Tb*NDT and its comparison with the hexameric assemblies of *Lh*PDT and *Ll*NDT revealed that the stabilization of these latter higher order oligomers demands a long α3 helix and consequently a long β2-α3 connecting loop of the subunits (see Discussion for details). The much shorter α3 helix and β2-α3 connecting loop of *Lm*PDT together with the location of α1 helix and the presence of the β6-α6 loop from the neighbor *Lm*PDT subunit results in a different architecture of the substrate-binding pocket when compared to *Lh*PDT or *Ll*NDT. Yet this novel arrangement has minor consequences in the internal volume of the active sites as determined with the CASTp server (Dundas et al. 2006), 810 $Å^3$ in *Lm*PDT versus 870 $Å^3$ in *Lh*NDT or 730 $Å^3$ *Ll*NDT, respectively. Curiously, these figures contrast with *Tb*NDT, which has a larger pocket (1130 $Å^3$). This difference can be attributed to


**Fig. 2** Amino acid sequence alignment of *Lm*PDT with its closest homologs. *Lm*PDT shares 67% sequence identity to the 2′-deoxyribosyltransferase from *Trypanosoma brucei* (*Tb*NDT), 18% to the 2′-deoxyribosyltransferase from *Lactobacillus leichmannii* (*Ll*NDT), and 13% to the 2′-deoxyribosyltransferase type I from *Lactobacillus helveticus* (*Lh*PDT). Secondary structural elements in *Lm*PDT are indicated as *orange arrows* (β-strands) and *green cylinders* (α helices). Amino acids color code: *red*, highly conserved positions; *white*, conserved positions

the specific conformation of the β2-α3 connecting loop: thus, whereas in *Lm*PDT this loop is directed towards the pocket, in *Tb*NDT it protrudes to the bulk solvent (Bosch et al. 2006) (Fig. S2 and supplementary video 1). The poor electron density of the side chains of some residues from this loop in *Lm*PDT (Asp43 to Ala46) suggests that this region is flexible and may play a role in substrate binding (see below).

The long β6-α6 loop of *Lm*PDT not only covers the substrate-binding pocket of the associated subunit but also contains residues that probably participate in substrate binding such as Asn128. In close proximity to this latter residue is situated Glu121, which occupies an equivalent position to the carboxyl group of the C-terminal Tyr157 that has been shown to play an important catalytic role (Anand et al. 2004).

## 2′-Deoxyadenosine complex

With a view to understanding the binding of a nucleoside at the active site of *Lm*PDT, the natural substrate 2′-deoxyadenosine (dAdo) was placed into the active site of the enzyme by means of docking and molecular dynamics (MD) protocols (see Computational methods in Materials and Methods). Briefly, the loop 43-46 was allowed to move freely along the MD simulation whereas a force constant of 5 kcal $mol^{-1}$ $Å^{-2}$ was applied to positional restrain the rest of the Cα atoms of the protein. In the resulting equilibrated structure, the loop 43-48 moves towards the bulk solvent, with the Asp43 side chain adopting a conformation that mimics the Glu50 side chain of *Tb*NDT (Fig. 3a). The interaction pattern shown in this figure reveals that the 2′-deoxyribosyl moiety of the deoxynucleoside is recognized by the side chains of the residues Asp79, Asn128, Glu85 (catalytic residue that is positioned by Tyr8), and Asn56 that participate in a dense network of hydrogen bonds (Fig. 3a). Complementary, whereas the adenine is recognized by the side chain of Asn56 similarly to Asp75 in *Lh*PDT, the amino group 6-$NH_2$ of the adenine interacts with the side chain of Glu121# in analogy to the carboxylate of the C-terminal Tyr in *Lh*PDT (Anand et al. 2004), as indicated before.

The crystal structure of *Lm*PDT reveals a glycerol molecule in each active site of the enzyme, in a location that superposes well with part of the 2′-desoxyribose ring of the in silico complex with dAdo (Fig. 3b). In particular, the oxygen atoms of the glycerol molecule superimpose almost perfectly with the O3′, O4′, and O5′ atoms of the 2′-deoxyribose and establish H-bonds with the side chains of Asp79, Glu85, similarly to the complex with dAdo.

## Catalytic activity

The 2′-deoxyribosyltransferase activity of *Lm*PDT was measured for a panel of donors (Urd, Ino, Ado, dUrd, dIno, dAdo, and dGuo) and acceptors (Ura, Hyp, Ade, and Gua) (specific activities summarized in Table 2). According to the experimental data, *Lm*PDT should be classified as 2′-deoxyribosyltransferase type I since it catalyzed the transfer of 2′-deoxyribose exclusively between purine bases. It did not interchange bases between ribonucleosides and no activity was detected for the transglycosylation reaction between pyrimidine nucleobase as donors and/or acceptors.

It is noteworthy that *Lm*PDT shows much higher specific activities than other reported type I NDTs under similar enzymatic assay conditions (Table 2). For instance, for the biosynthesis of 2′-deoxyadenosine from 2′-deoxyinosine and adenine, the specific activity showed by *Lm*PDT (73.1 μmol $min^{-1}$ $mg^{-1}$) was 2.2, 1.7, 20, and 67 times higher than the values of *Ll*NDT (42.2 μmol $min^{-1}$ $mg^{-1}$) (Becker and Brendel 1996), *L. reuteri* NDT (34 μmol $min^{-1}$ $mg^{-1}$) (Fernández-Lucas et al. 2010),

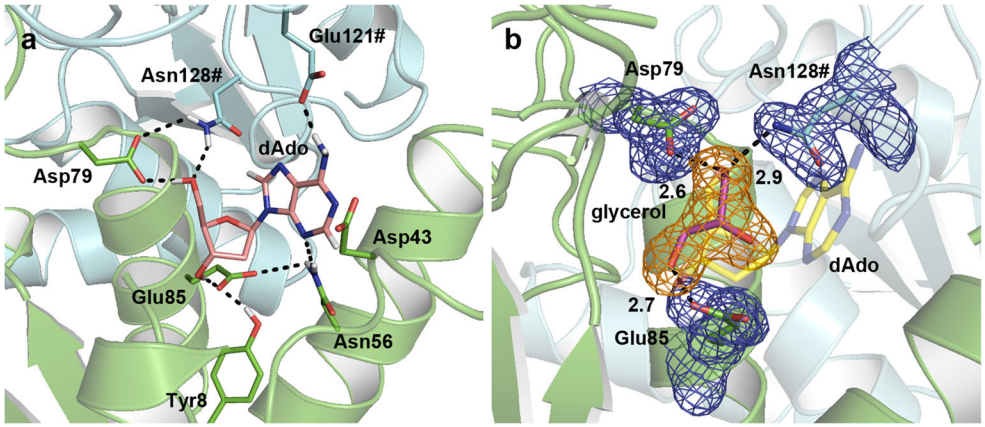


**Fig. 3** Active site of *Lm*PDT. **a** In silico complex of 2′-deoxyadenosine (dAdo) bound to *Lm*PDT. Residues from both subunits of *Lm*PDT would participate in dAdo-binding, in particular, Asn56, Asp79, and Glu85 from one subunit and Glu121# and Asn128# from the other. Tyr8 would properly orientate the Glu85 side chain to interact with the substrate. **b** Crystal structure of the complex of *Lm*PDT with glycerol bound within the active site. Oxygen atoms of the glycerol molecule occupy almost identical positions as those predicted for the O3′, O4′, and O5′ atoms from the 2′-deoxyribose ring of dAdo (as *semitransparent stick* model). The $2F_o$-$F_c$ electron density map is contoured at 1σ. Putative H-bonds are shown as *dashed lines*. Distances are in angstrom

*Lactococcus lactis* NDT (3.6 μmol $min^{-1}$ $mg^{-1}$) (Yukiko et al. 2007), and *Lactobacillus fermentum* NDT (1.1 μmol $min^{-1}$ $mg^{-1}$) (Kaminski et al. 2008), respectively. The specific activities of *Lm*PDT were approximately equal regardless of the donor, whereas a lower activity was found for guanine as acceptor (Table 2). This finding was corroborated using the same concentration of acceptor and 2′-fluoro-2′-deoxyadenosine as donor.

Structural insights explaining the lower activity of *Lm*PDT towards guanine as acceptor when compared to adenine and hypoxanthine were obtained by analyzing the substrate-binding site with the program cGRILL (Cortés-Cabrera et al. 2015). With this aim, affinity maps for the $NH_4^+$ and oxygen probes were calculated for the putative ribosylated form of the enzyme in the absence of the nucleobase. Then, the three nucleobases were manually docked into the active site of *Lm*PDT (Fig. 4). Whereas Ade and Hyp would orientate their attacking nitrogen N9 into a favorable region according to the affinity map obtained with the O probe (red mesh), Gua in its near-attack conformation would orientate its carbonyl oxygen and the exocyclic amine group into unfavorable affinity regions; hence, formation of 2′-deoxyguanosine would be impeded on energetic considerations.

**Table 2** Synthesis of natural nucleosides catalyzed by *LmPDT*. Specific activities (units/mg protein) of *Lm*PDT compared with *Lh*PDT (Kaminski 2002) and *Bb*PDT (Lawrence et al. 2009)

| | *Lm*PDT | | | *Lh*PDT | | | *Bb*PDT | | | |
|---|---|---|---|---|---|---|---|---|---|---|
| Acceptor | Ade[a] | Gua[b] | Hyp[a] | Ade[a] | Gua[b] | Hyp[a] | Ade[a] | Gua[b] | Hyp[a] |
| Donor | | | | | | | | | | |
| dAdo | – | 13.8 | 75.4 | – | n.p. | 0.06 | – | 0.09 | 0.02 |
| dGuo | 52.7 | – | 68.6 | 0.05 | – | 0.05 | 0.08 | – | 0.02 |
| dIno | 73.1 | 14.5 | – | 0.08 | n.p. | – | 0.04 | 0.04 | – |

*n.p.* not performed

[a] Reaction conditions: 0.3 μg of enzyme in 40 μL at 40 °C, 5 min. (Substrates) = 10 mM, 50 mM MES buffer, pH 6.5

[b] Reaction conditions, 0.3 μg of enzyme in 40 μL at 40 °C, 5 min. (Substrates) = 1 mM in 50 mM phosphate buffer, pH 8.5

## Temperature, pH, and ionic strength dependence of *Lm*PDT catalytic activity

The effects of temperature, pH, and ionic strength dependence on the stability and activity of the enzyme were studied to determine the optimal operating conditions of the enzyme (Fig. 5). On the one hand, the effect of temperature on *Lm*PDT activity was examined by measuring the biosynthesis of dAdo from dGuo and Ade in the temperature range from 20 to 90 °C using standard assay conditions. As shown in Fig. 5a, high activity (≥ 90%) was achieved between 30 and 70 °C, with a maximum value at 40–50 °C. On the other hand, the activity of *Lm*PDT was also examined in the pH range from 4 to 10 under the same standard assay conditions (Fig. 5b). *Lm*PDT displays a great operational activity in a broad range of pH (higher than 90% in a pH range from 5.5 to 8.5, and higher than 80% in a pH range from 5 to 9). Finally, *Lm*PDT retains its catalytic activity at high salt concentrations (90% of activity remains at 0.5 M NaCl) (Fig. 5c).

## Enzymatic stability

The stability of a biocatalyst is defined as the time during which it retains 50% of its initial activity and could be affected by

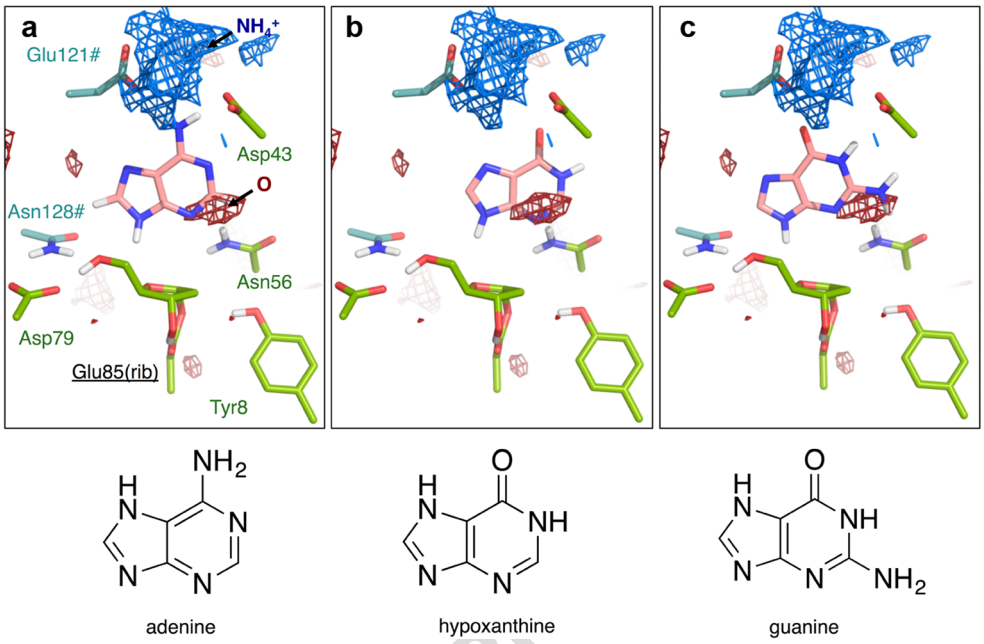


**Fig. 4** Affinity maps calculated for the $NH4^+$ (*blue mesh*) and oxygen (*red mesh*) probes using the program cGRILL (29) within the active site of *Lm*PDT with **a** adenine, **b** hypoxhantine, or **c** guanine considered as acceptors

environmental conditions such as pH and temperature. In this sense, the temperature and pH effect on *Lm*PDT stability was evaluated by incubating the enzyme for 48 h at 40 °C at different pH conditions (6.5, 8.5, and 10) (Fig. 5d). Regarding the latter parameter, unexpectedly, alkaline environments (pH 8–10) do not inactivate the enzyme during the assayed period.

## Synthesis of non-natural nucleosides

The synthetic scope of *Lm*PDT was evaluated for the glycosyltransfer reaction between several non-natural nucleosides, such as 2′-fluoro-2′-deoxy-, 2′,3′-dideoxy-, and arabinosyl nucleosides using adenine, guanine, and hypoxanthine under

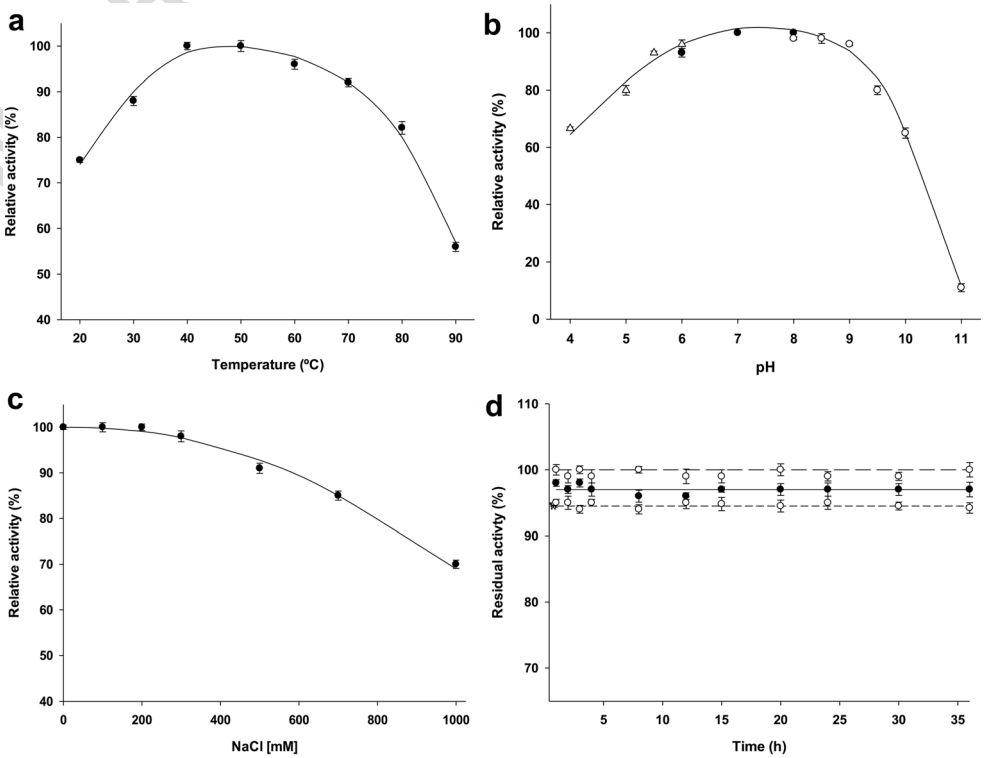


**Fig. 5** Biochemical characterization of *Lm*PDT. **a** Effect of temperature on *LmPDT* activity (*black circle*). **b** Effect of pH on *Tt*HGXPRT activity, *white triangle* sodium acetate 50 mM (pH 4–6), *black circle* sodium phosphate 50 mM (pH 6–8), *white circle* sodium borate 50 mM (pH 8–10). **c** Effect of ionic strength on *Tt*HGXPRT activity (*black circle*). **d** Thermal inactivation of *Tt*HGXPRT at 60 °C in sodium borate 50 mM (pH 8–10), *white triangle* pH 8, *white circle* pH 9, and *black circle* pH 10

different assay conditions (Table 3 and Fig. S1). In contrast to the natural substrates, mild conversions were detected in HPLC after 4 and 24 h of reaction. Among the tested donors, 2'F-Ino afforded the highest yields in the transglycosylation to adenine and guanine. To a lesser extent, a similar reactivity was obtained for the dideoxynucleosides ddA and ddI as donors. Finally, when using the arabinosyl nucleosides (ara A, G, and H) as source of glycosyl, the activity of *Lm*PDT was low.

## Discussion

Purine nucleotides are essential compounds in all living organisms. They can be synthesized by the de novo and/or the so-called "salvage" pathways. Unlike their mammalian hosts, most parasites studied lack the pathways for de novo purine biosynthesis and they rely on the salvage pathways to meet their purine demands. Since the final objective of de novo synthesis is the production of inosine-5′-monophosphate (IMP), the absence of this metabolic route demands an efficient alternative to synthesize IMP (el Kouni 2003). Most parasites circumvent this problem by an efficient and complex purine salvage pathway, formed by a substantial number of enzymes, such as nucleoside hydrolases, nucleoside phosphorylases, nucleoside kinases, 2′-deoxyribosyltransferases, deaminases, or phosphoribosyltransferases with the potential to be involved in cleaving, assembling, and interconverting scavenged nucleosides and nucleobases in parasites (el Kouni 2003).

Since inosine and xanthosine kinases are detected in a low amount in *Leishmania* species (Datta et al. 2008), phosphorylation of inosine seems to be a non-efficient way for the IMP synthesis. In addition, adenosine deaminase, which catalyzes the conversion of adenosine to inosine, is only present in *Leishmania* amastigotes (Datta et al. 2008). Due to this, ribophosphorylation of hypoxanthine by hypoxanthine-guanine phosphoribosyltransferase (HGPRT) seems to be the most effective synthetic route for IMP synthesis.

One of the processes of purine recycling entails the removal of the ribose or 2′-deoxyribose moiety from purine nucleosides through the cleavage of C-N glycosidic bond. This process is accomplished by at least three types of enzymes: purine nucleoside phosphorylases, PNPs (EC 2.4.2.1); purine nucleoside hydrolases, NHs (EC 3.2.2.1); or nucleoside deoxyribosyltransferases, NDTs (EC 2.4.2.6). The presence of PNPs is not reported in *Leishmania*, and NHs are strictly specific for ribonucleosides, with negligible activity over 2′-deoxyribonucleosides (Shi et al. 1999; Versées and Steyaert 2003), so NDTs is the only effective way to recover hypoxanthine. In addition, several lines of evidence suggest a specific role of PDT in the eradication of dIno from the cellular nucleoside pool by converting dIno to hypoxanthine, which can then be recycled to IMP by hypoxanthine phosphoribosyltransferase (Fresco-Taboada et al. 2013; Kaminski 2002; Steenkamp and Hälbich 1992).

Here, we have reported a thorough functional and structural characterization of the purine 2′-deoxyribosyltransferase of *L. mexicana* (*Lm*PDT). Analysis of the *Lm*PDT structure and sedimentation velocity experiments reveals that the protein is a dimer similarly to *Tb*NDT but in contrast to the bacterial, homolog enzymes *Ll*NDT and *Lh*PDT, which are homohexamers (trimers of dimers), revealing a marked pleomorphism within this family of proteins. The hexameric assembly of *Ll*NDT and *Lh*NDT belongs to the D3 dihedral group (Goodsell and Olson 2000) since it contains a threefold rotational symmetry axis perpendicular to a twofold axis (Fig. 6). Molecular interfaces between subunits related by the twofold axis result from the antiparallel stacking of α4 and α4# helices and the penetration of the α6 helix and the three C-terminal residues between the α3# and α4# helices (Fig. 6a). Not surprisingly, these interfaces are essentially conserved in the four proteins (*Lm*PDT, *Tb*NDT, *Lh*PDT, and *Ll*NDT) since they are responsible for the built-up of the dimeric assembly, the basic catalytic unit of this family of proteins (Armstrong et al. 1996) (Fig. 6b). Nonetheless, an important difference is observed between hexameric and dimeric enzymes regarding these common interfaces. In particular, similar intersubunit interactions identified in *Lh*PDT and *Ll*NDT involving the C-terminal residues are observed neither in *LmPDT* nor in *Tb*NDT what is remarkable since the carboxylate group of the C-terminal residue of *Lh*PDT has been shown to play an important catalytic role (Anand et al. 2004). As indicated above, this role is now probably played by Glu121#, which occupy a similar location in *Lm*PDT. Conversely, the main contacting interfaces between subunits related by the perpendicular threefold axis in *Ll*NDT and *Lh*PDT are formed by α3 helix that packs against a long C-terminal, irregular segment of the neighbor subunit (comprised by residues 155–162 in *Lh*NDT and 146–151 in *Ll*NDT) and only for *Lh*PDT also by the side-

**Table 3** Synthesis of nucleoside analogues catalyzed by *Lm*PDT

| Acceptor | Ade[n] | | Gua[b] | | Hyp[a] | |
|---|---|---|---|---|---|---|
| | 4 h | 24 h | 4 h | 24 h | 4 h | 24 h |
| Donor | | | | | | |
| ddA | – | – | 10% | 52% | 11% | 57% |
| ddI | 46% | 20% | 20% | 6% | – | – |
| ara A | – | – | n.p. | 10% | n.p. | 9% |
| ara G | n.p. | 30% | – | – | n.p. | 16% |
| ara H | n.p. | 25% | – | 6% | – | – |
| 2'F-Ino | 15% | 57% | 18% | 61% | – | – |

*n.p.* not performed

[a] Reaction conditions, 3 μg of enzyme in 40 μL at 40 °C, 4–24 h. (Substrates) = 1 mM, 50 mM MES buffer, pH 6.5

[b] Reaction conditions, 3 μg of enzyme in 40 μL at 40 °C, 4–24 h. (Substrates) = 1 mM, 50 mM sodium borate 50 mM, pH 8.5

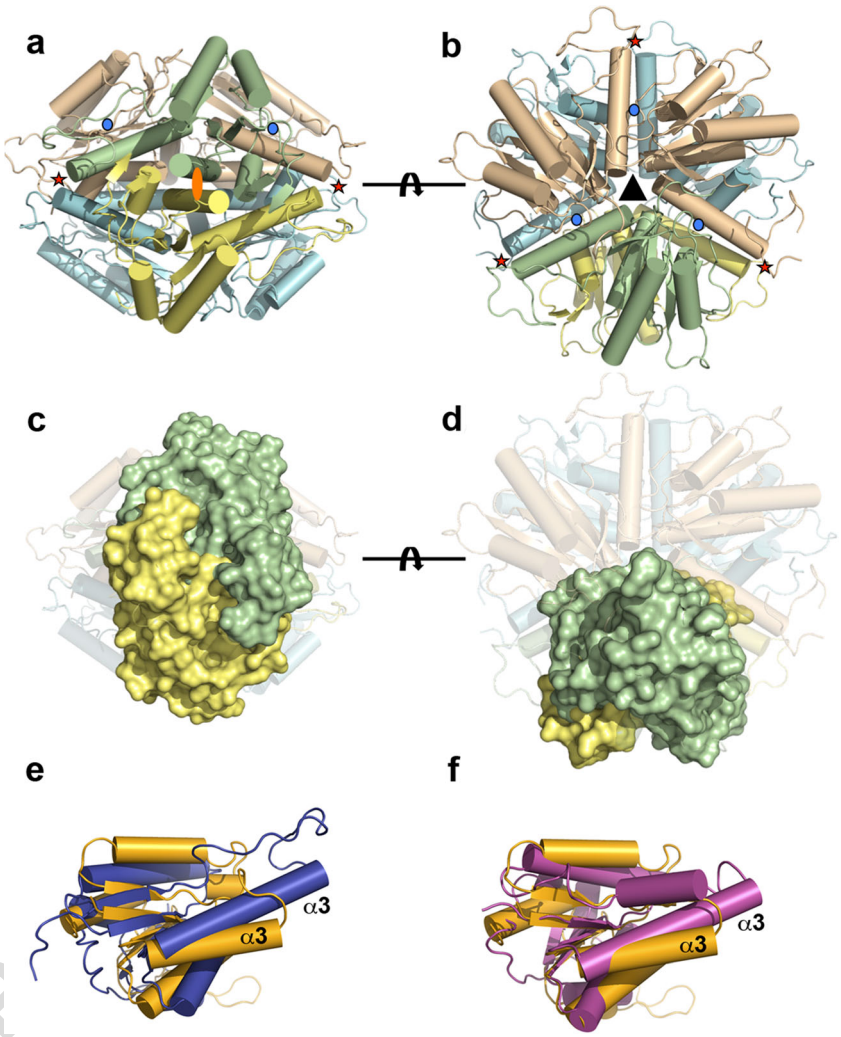


**Fig. 6** Molecular symmetry of the hexameric assembly of *Lactobacillus helveticus* 2′-deoxyribosyltransferase (*Lh*PDT) and structural comparison with the *Lm*PDT subunit. **a**, **b** Orthogonal views of the hexamer of *Lh*PDT. The twofold molecular symmetry axis is shown as an *orange ellipse* and the threefold axis as a *black triangle*; both axes are perpendicular to the plane of the figure. *Blue circles* indicate the contacting regions between subunits related by the threefold symmetry axis and *red stars* contacting regions not related by the molecular symmetry (see text for details). To facilitate the interpretation and also the comparison with *Lm*PDT, a dimer of *Lh*PDT is highlighted with *yellow* and *green* subunits. **c**, **d** The same views as before but indicating the relative position of the *Lm*PDT dimer (as *surface model*; one subunit *green* and the other *yellow*). Three-dimensional superposition of the *Lm*PDT subunit (orange) with the *Lh*PDT subunit (*blue*) (**e**) and *Ll*NDT (*magenta*) (**f**). Helices are shown as *solid cylinders* and β-strands as *arrows*. The figures have been prepared with PyMOL (DeLano 2002)

by-side interaction between the β2 strand and the four N-terminal residues of the accompanying subunit. As expected, key structural elements involved in trimer stabilization are not present in *LmPDT* (Fig. 6d).

Within dihedral oligomers, novel interfaces may appear between subunits not related by rotational symmetry (Goodsell and Olson 2000). In the case of *Ll*NDT and *Lh*PDT hexamers, this type of contacts is represented by interfaces between elements that belong neither to the same dimer nor to the same trimer. These types of contacts are exemplified here by interactions between the N-terminal ends of α3 helices from subunits not related by the rotational, molecular symmetry (Fig. 6a, c). This is consistent with our observation that α3 helices from the hexameric enzymes are much longer than the equivalent from dimeric ones. This observation suggests that from a structural point of view, the stabilization of the hexameric assembly of *Ll*NDT and *Lh*PDT demands a long β2-α3 connecting loop (*Lh*PDT; Fig. 6E), or connecting region (*Ll*NDT; Fig. 6F), derived from their much longer α3 helices. We believe that this is relevant because this region is located above the substrate-binding pockets of *Ll*NDT and *Lh*NDT and plays an important role in the definition of the substrate specificity of class I versus class II *N*-deoxyribosyltransferases (Anand et al. 2004). Since the much shorter connecting loop of *Lm*PDT or *Tb*NDT enzymes does not cover their active sites, its specific functional role in *Ll*NDT and *Lh*PDT should be understood as an emergent feature that most probably results from the interplay between optimization of interactions within the higher order oligomeric assemblies endowed with D3 symmetry and their catalytic activity.

The poor electron density of the side chains of some residues from the much shorter β2-α3 loop in *Lm*PDT (Asp43 to Ala46) suggests that it is flexible. Our combined crystallographic and in silico studies suggest that the dynamic features of this loop may be important in substrate binding. Hence, whereas the conformation of this loop in the absence of bound substrate is revealed by the structure of *Lm*PDT, our molecular dynamics studies suggest that the conformation of this loop with dAdo bound within the active site progresses towards the conformation found in the *Tb*NDT structure (Fig. S2 and supplementary video 1).

The calculated specific activity values of *Lm*PDT are much higher than those reported for other PDTs, such as *Lh*PDT or PDT from *Borrelia burgdorferi*, *Bb*PDT (between 100- or 4000-fold higher in the same experimental conditions; Table 2). A putative explanation for these higher activities could be found in the essential physiological role of nucleoside deoxyribosyltransferases in the purine salvage pathway in *Leishmania* species since, as described above, these enzymes constitute the only effective way to recover hypoxanthine in parasites. By contrast, other microorganisms have alternative synthetic routes for IMP synthesis: for instance, in *Borrelia burgdorferi*, adenosine deaminases and deoxynucleoside kinases have been reported (Lawrence et al. 2009), and in *L. helveticus* 2′-deoxyribosyltransferases (NDTs and PDTs), as well as an adenosine deaminase have been identified (Kaminski 2002).

Yet the most remarkable biochemical feature of *Lm*PDT is its stability at high pH and temperature values; in fact, as far as we know, it is the first time that this high tolerance to alkaline conditions is reported for an NDT. We believe that this is relevant since one of the most limiting factors for the industrial synthesis of purine nucleosides is the low solubility of some purine bases (guanine, hypoxanthine, and/or xanthine) in the reaction medium. Our results suggest that *Lm*PDT may be an interesting alternative to circumvent this problem.

Furthermore, this non-usual stability at high pH values entails another significant advantage. Since enzyme immobilization is an essential requirement for the use of enzymes as industrial biocatalysts, enzyme stability under immobilization conditions is necessary. Covalent immobilization of proteins usually occurs via multipoint attachment through the region with higher density of primary amino groups, especially with ε-$NH_2$ from lysine residues (Mateo et al. 2007). Due to this, covalent immobilization techniques usually employ long reaction times (2–24 h) and alkaline conditions (pH 8–10). In this way, the exceptional stability displayed by *Lm*PDT in alkaline conditions suggests that it could be efficiently immobilized.

The only precedent of an enzyme-based synthesis of 2′-deoxyguanosine was described by Okuyama et al. (2003) and was based on the multi-enzymatic system *Lh*NDT/*Ec*ADA. Regarding to its potential applicability in the industrial synthesis of nucleoside analogues, it is obvious that the one-step action of *Lm*PDT is a priori a simpler scenario than the coupling system *Lh*NDT/*Ec*ADA since the latter would require the co-immobilization of the *Lh*NDT and *Ec*ADA enzymes to perform the reaction.

As a proof of concept, *Lm*PDT was employed as biocatalyst for the synthesis of different therapeutic nucleoside analogues (Table 3) (Fig. S1), such as 2′,3′-dideoxyguanosine (ddG—a selective inhibitor of the replication of human immunodeficiency virus in vitro and an active antihepadnavirus nucleoside analogue) (Bondoc et al. 1992), 2′,3′-dideoxyinosine (ddI, didanosine, a potent inhibitor of HIV replication) (World Health Organization 2011), 9-β-D-arabinofuranosyl adenine (ara A, vidarabine, not only an antiviral drug which is active against herpes simplex and varicella zoster viruses, but a potential precursor of fludarabine and clofarabine, approved FDA drugs for the cancer treatment) (De Clerq 2005a, b; Galmarini et al. 2002; Parker 2009; Wilhelmus 2015), 9-β-D-arabinofuranosyl guanine (ara G, precursor of nelarabine, approved FDA drugs for the cancer treatment of T cell malignancies) (Parker 2009), and 2′-fluoro-2′-deoxyguanosine (2'F-dGuo, an anti-influenza virus agent) (Tuttle et al. 1993). Although in low conversions compared to the natural substrates, we detected the expected, final products. This is remarkable since to date no wild-type NDT has been described to perform the synthesis of 2′,3′-dideoxyribonucleosides despite the fact that wild-type NDTs from *L. helveticus* (Carson and Wasson 1988), *L. fermentum*, and *L. leichmannii* (Kaminski et al. 2008) recognize this type of molecules with very low affinity. Finally, our results also reveal that *Lm*PDT bind 2'F-dGuo and arabinosyl nucleosides. This means that the binding site tolerates the presence of a fluorine atom or a hydroxyl group at position 2′ of the sugar ring. All these particularities, together with its high activity and stability in alkaline conditions, make *Lm*PDT the first reported NDT able to catalyze the synthesis of 2'F-dGuo, ara G and ara H.

**Acknowledgements** This work was supported by grants from the Spanish Ministerio de Economía y Competitividad (BFU2010-17929/BMC to J.M.M. and SAF2015-64629-C2-2-R to F.G.), and SAN151610 from the Santander Foundation (to J.F.L.). J.M.M. thanks the synchrotron ALBA for the access to the radiation source.

**Compliance with ethical standards**

**Conflict of interest** The authors declare that they have no conflict of interest.

**Ethical approval** This article does not contain any studies with human participants or animals by any of the authors.

**Funding** This work was supported by grants from the Spanish Ministerio de Economía y Competitividad (BFU2010-17929/BMC to J.M.M. and SAF2015-64629-C2-2-R to F.G.), and SAN151610 from the Santander Foundation (to J.F.L.).

## References

Adams PD, Afonine PV, Bunkóczi G, Chen VB, Davis IW, Echols N, Headd JJ, Hung LW, Kapral GJ, Grosse-Kunstleve RW, McCoy AJ, Moriarty NW, Oeffner R, Read RJ, Richardson DC, Richardson JS, Terwilliger TC, Zwart PH (2010) PHENIX: a comprehensive Python-based system for macromolecular structure solution. Acta Crystallogr Sect D Biol Crystallogr 66:213–221

Afonine PV, Grosse-Kunstleve RW, Echols N, Headd JJ, Moriarty NW, Mustyakimov M, Terwilliger TC, Urzhumtsev A, Zwart PH, Adams PD (2012) Towards automated crystallographic structure refinement

with phenix.refine. Acta Crystallogr Sect D Biol Crystallogr 68: 352–367

Anand R, Kaminski PA, Ealick SE (2004) Structures of purine 2′-deoxyribosyltransferase, substrate complexes, and the ribosylated enzyme intermediate at 2.0 Å resolution. Biochemistry 43:2384–2393

Anandakrishnan R, Aguilar B, Onufriev AV (2012) H++ 3.0: automating pK prediction and the preparation of biomolecular structures for atomistic molecular modeling and simulations. Nucleic Acids Res 40:W537–W541

Armstrong SR, Cook WJ, Short SA, Ealick SE (1996) Crystal structures of nucleoside 2′-deoxyribosyltransferase in native and ligand-bound forms reveal architecture of the active site. Structure 4:97–107

Becker J, Brendel M (1996) Rapid purification and characterization of two distinct N-deoxyribosyltransferases of *Lactobacillus leichmannii*. Biol Chem Hoppe Seyler 377:357–362

Bondoc LL, Ahluwalia G, Cooney DA, Hartman NR, Johns DG, Fridland A (1992) Metabolic pathways for the activation of the antiviral agent 2′,3′-dideoxyguanosine in human lymphoid cells. Mol Pharmacol 42:525–530

Boryski J (2008) Reactions of transglycosylation in the nucleoside chemistry. Curr Org Chem 12:309–325

Bosch J, Robien MA, Mehlin C, Boni E, Riechers A, Buckner FS, Van Voorhis WC, Myler PJ, Worthey EA, DeTitta G, Luft JR, Lauricella A, Gulde S, Anderson LA, Kalyuzhniy O, Neely HM, Ross J, Earnest TN, Soltis M, Schoenfeld L, Zucker F, Merritt EA, Fan E, Verlinde CLMJ, Hol WGJ (2006) Using fragment cocktail crystallography to assist inhibitor design of *Trypanosoma brucei* nucleoside 2-deoxyribosyltransferase. J Med Chem 49:5939–5946

Brown PH, Schuck P (2006) Macromolecular size-and-shape distributions by sedimentation velocity analytical ultracentrifugation. Biophys J 90:4651–4661

Carson DA, Wasson DB (1988) Synthesis of 2′,3′-dideoxynucleosides by enzymatic trans-glycosylation. Biochem Biophys Res Commun 155:829–834

Case DA, Babin V, Berryman JT, Betz RM, Cai Q, Cerutti DS, Cheatham TE, Darden TA, Duke RE, Gohlke H, Goetz AW, Gusarov S, Homeyer N, Janowski P, Kaus J, Kolossváry I, Kovalenko A, Lee TS, LeGrand S, Luchko T, Luo R, Madej B, Merz KM, Paesani F, Roe DR, Roitberg A, Sagui C, Salomon-Ferrer R, Seabra G, Simmerling CL, Smith W, Swails J, Walker RC, Wang J, Wolf RM, Wu X, Kollman PA (2014) AMBER 14. University of California, San Francisco

Cortés-Cabrera Á, Gago F, Morreale A (2015) A computational fragment-based *de novo* design protocol guided by ligand efficiency indices. In: Klon AE (ed) Fragment-based methods in drug discovery. Springer, New York, pp 89–100

Datta AK, Datta R, Sen B (2008) In: Majumder HK (ed) Drug targets in Kinetoplastid parasites. Springer New York, New York, NY., pp 116–132

De Clercq E (2005a) Antiviral drug discovery and development: where chemistry meets with biomedicine. Antivir Res 67:56–75

De Clercq E (2005b) Recent highlights in the development of new antiviral drugs. Curr Opin Microbiol 8:552–560

DeLano WL (2002) The PyMOL molecular graphics system. DeLano Scientific, San Carlos

Dundas J, Ouyang Z, Tseng J, Binkowski A, Turpaz Y, Liang J (2006) CASTp: computed atlas of surface topography of proteins with structural and topographical mapping of functionally annotated residues. Nucleic Acids Res 34:W116–W118

el Kouni MH (2003) Potential chemotherapeutic targets in the purine metabolism of parasites. Pharm Ther 99:283–309

Emsley P, Lohkamp B, Scott WG, Cowtan K (2010) Features and development of Coot. Acta Crystallogr Sect D Biol Crystallogr 66:486–501

Evans PR (2011) An introduction to data reduction: space-group determination, scaling and intensity statistics. Acta Crystallogr Sect D Biol Crystallogr 67:282–292

Fernández-Lucas J, Acebal C, Sinisterra JV, Arroyo M, de la Mata I (2010) *Lactobacillus reuteri* 2′-deoxyribosyltransferase, a novel biocatalyst for tailoring of nucleosides. Appl Environ Microbiol 76: 1462–1470

Fernández-Lucas J, Fresco-Taboada A, de la Mata I, Arroyo M (2012) One-step enzymatic synthesis of nucleosides from low water-soluble purine bases in non-conventional media. Bioresour Technol 115:63–69

Fresco-Taboada A, de la Mata I, Arroyo M, Fernández-Lucas J (2013) New insights on nucleoside 2′-deoxyribosyltransferases: a versatile biocatalyst for one-pot one-step synthesis of nucleoside analogs. Appl Microbiol Biotechnol 97(9):3773–3785

Galmarini CM, Mackey JR, Dumontet C (2002) Nucleoside analogues and nucleobases in cancer treatment. Lancet Oncol 3:415–424

Gill SC, Von Hippel PH (1989) Calculation of protein extinction coefficients from amino acid sequence data. Anal Biochem 182:319–326

Goodsell DS, Olson AJ (2000) Structural symmetry and protein function. Annu Rev Biophys Biomol Struct 29:105–153

Holm L, Rosenström P (2010) Dali server: conservation mapping in 3D. Nucleic Acids Res 38:W545–W549

Kabsch W (2010) Integration, scaling, space-group assignment and post-refinement. Acta Crystallogr Sect D Biol Crystallogr 66:133–144

Kaminski PA (2002) Functional cloning, heterologous expression, and purification of two different N-deoxyribosyltransferases from *Lactobacillus helveticus*. J Biol Chem 277:14400–14407

Kaminski PA, Dacher P, Dugue L, Pochet S (2008) In vivo reshaping the catalytic site of nucleoside 2 '-deoxyribosyltransferase for dideoxy- and didehydronucleosides via a single amino acid substitution. J Biol Chem 283:20053–20059

Klett J, Núñez-Salgado A, Dos Santos HG, Cortés-Cabrera A, Perona A, Gil-Redondo R, Abia D, Gago F, Morreale A (2012) MM-ISMSA: an ultrafast and accurate scoring function for protein–protein docking. J Chem Theory Comput 8:3395–3408

Krissinel E, Henrick K (2007) Inference of macromolecular assemblies from crystalline state. J Mol Biol 372:774–797

Laue TM, Shah BD, Ridgeway TM, Pelletier SL (1992) Computer-aided interpretation of analytical sedimentation data for proteins. In: Harding SE, Rowe AJ, Horton JC (eds) Analytical ultracentrifugation in biochemistry and polymer science. Royal Society of Chemistry, UK, pp 90–125 Q3

Lawrence KA, Jewett MW, Rosa PA, Gherardini FC (2009) *Borrelia burgdorferi* bb0426 encodes a 2′-deoxyribosyltransferase that plays a central role in purine salvage. Mol Microbiol 72:1517–1529

Lewkowicz E, Iribarren A (2006) Nucleoside phosphorylases. Curr Org Chem 10:1197–1215

Mateo C, Palomo JM, Fernandez-Lorente G, Guisan JM, Fernandez-Lafuente R (2007) Improvement of enzyme activity, stability and selectivity via immobilization techniques. Enzym Microb Technol 40:1451–1463

McCoy AJ (2007) Solving structures of protein complexes by molecular replacement with Phaser. Acta Crystallogr Sect D Biol Crystallogr 63:32–41

Mikhailopulo IA (2007) Biotechnology of nucleic acid constituents-state of the art and perspectives. Curr Org Chem 11:317–335

Müller M, Hutchinson LK, Guengerich FP (1996) Addition of deoxyribose to guanine and modified DNA bases by *Lactobacillus helveticus* trans-N-deoxyribosylase. Chem Res Toxicol 9:1140–1144

Okuyama K, Shibuya S, Hamamoto T, Noguchi T (2003) Enzymatic synthesis of 2′-deoxyguanosine with nucleoside deoxyribosyltransferase-II. Biosci Biotechnol Biochem 67:989–995

Parker WB (2009) Enzymology of purine and pyrimidine antimetabolites used in the treatment of cancer. Chem Rev 109:2880–2893

Robak T, Lech-Maranda E, Korycka A, Robak E (2006) Purine nucleoside analogs as immunosuppressive and antineoplastic agents:

mechanism of action and clinical activity. Curr Med Chem 13:3165–3189

Sánchez-Murcia PA, Bueren-Calabuig JA, Camacho-Artacho M, Cortés-Cabrera Á, Gago F (2016) Stepwise simulation of 3, 5-dihydro-5-methylidene-4 H-imidazol-4-one (MIO) biogenesis in histidine ammonia-lyase. Biochemistry 55:5854–5864

Shi W, Schramm VL, Almo SC (1999) Nucleoside hydrolase from Leishmania major: cloning, expression, catalytic properties, transition state inhibitors, and the 2.5 Å structure. J Biol Chem 274:21114–21120

Short SA, Armstrong SR, Ealick SE, Porter DJT (1996) Active site amino acids that participate in the catalytic mechanism of nucleoside 2′-deoxyribosyltransferase. J Biol Chem 271:4978–4987

Steenkamp DJ, Hälbich TJF (1992) Substrate specificity of the purine-2′-deoxyribonucleosidase of *Crithidia luciliae*. Biochem J 287:125–129

Touw WG, Baakman C, Black J, te Beek TA, Krieger E, Joosten RP, Vriend G (2015) A series of PDB-related databanks for everyday needs. Nucleic Acids Res 43:D364–D368

Tuttle JV, Tisdale M, Krenitsky TA (1993) Purine 2′-deoxy-2′-fluororibosides as antiinfluenza virus agents. J Med Chem 36:119–125

Vanquelef E, Simon S, Marquant G, Garcia E, Klimerak G, Delepine JC, Cieplak FY, Dupradeau FY (2011) RED server: a web service for deriving RESP and ESP charges and building force field libraries for new molecules and molecular fragments. Nucleic Acids Res 39:W511–W517

Versées W, Steyaert J (2003) Catalysis by nucleoside hydrolases. Curr Opin Struct Biol 13:731–738

Wilhelmus KR (2015) Antiviral treatment and other therapeutic interventions for herpes simplex virus epithelial keratitis. Cochrane Database Syst Rev 1:CD00289

World Health Organization (2011) WHO model list of essential medicines: 17th list, March

Ye Y, Godzik A (2003) Flexible structure alignment by chaining aligned fragment pairs allowing twists. Bioinformatics 19:ii246–ii255

Yokozeki K, Tsuji T (2000) A novel enzymatic method for the production of purine-2′-deoxyribonucleosides. J Mol Catal B Enzym 10:207–213

Yukiko M, Taheharu M, Shigeru C (2007) Characterization of N-deoxyribosyltransferase from Lactococcus lactis subsp. Lactis. Biochim Biophys Acta 1774:1323–1330

# AUTHOR QUERIES

**AUTHOR PLEASE ANSWER ALL QUERIES.**

Q1. The sentence "Conversely, although in the active site of LmPDT..." was slightly modified. Please check if correct.
Q2. Please check whether in the references all species names are typeset in italics.
Q3. Please replace the country name with the city name for the publisher’s location.